Geometric Optics and Electromagnetic Models for Cylindrical Obstacles

D. Trappeniers, **R. G. Gonzàlez**, **E. van Lil**, and **A. van de Capelle**
K. U. Leuven, Belgium

Abstract—A software prediction tool called EPICS (Enhanced Propagation for Indoor Communications Systems) was developed at the ESAT-TELEMIC division of the K. U. Leuven in two versions: a Geometric Optics (GO) version and a Physical Optics (PO) version. However, like many other three-dimensional package, this can only determine the signal in an environment that can be decomposed into (ir)regular hexahedral obstacles (with 6 sides like rectangular blocks, cubes, etc.) or (complex) combinations of them. Although most of the real life environment can be approximated by these hexahedral obstacles, this might lead to some artefacts like periodic radar cross section variations, the need for multiple diffractions to calculate the signal behind a cylindrical obstacle, or reflections that are ignored (e. g., because the approximated side plane is positioned so that a reflection on that plane can not reach the receiver) is existing. To calculate the signal more accurately for those cases, we need to implement curved obstacles into EPICS. In a first step to achieve this goal, the introduction of cylindrical obstacles is investigated.

In this paper, the general strategy is discussed. The first step is to determine the different intermediate (i. e., penetration, reflection and diffraction) points on the ray between transmitter and receiver. Efficient computational routines have been written and tested for this purpose, mostly solving the problem first in two dimensions (projected in a plane perpendicular to the axis of the cylinder) and then transforming this solution to the three-dimensional problem. Once these intermediate points have been found, one can start with the computation of the electromagnetic field.

In the case of a penetration, the intermediate point(s) can be found very easily (crossing point(s) of a line and a circle) and the electromagnetic computations don't differ from the computations with hexahedral obstacles. For the reflection by a non perfectly conducting surface, the plane wave Fresnel reflection coefficients can be used. Also the finite thickness of the cylindrical walls can be taken into account, using internal (multiple) reflections, if the losses are high or the reflection coefficient of the wall is not to large.

For the diffractions, the two-dimensional geometric problem that needs to be solved to find the diffraction points is the determination of the tangent line to a circle (both from transmitter and receiver). Note that both can have two tangent lines, and one might have to match the two corresponding diffraction points. In this case, the electromagnetic computations for the vertical (i. e., field component parallel with the axis of the cylinder) and horizontal polarisation are done separately. An important issue in these computations is the convergence of the series used for the calculation of the field.

The reflection points on a cylindrical wall can not be found as easily as in the previous two cases. In general, an iterative process is required. This implies that the search for a good starting value is an important issue. Therefore some efficient computer programs were written to find firstly a good starting value of the Newton-Raphson iteration. As for the electromagnetic computations, one has to take into account that the caustics are transformed after the reflections and thus another amplitude factor has to be taken into account.

Although the described routines are not (yet) a part of the EPICS software, new routines based on Geometric Optics (GO) have been written and tested (in matlab) to predict penetration, reflection and diffraction of electromagnetic fields around cylindrical obstacles. This will be used to compute the effects of a curved airport terminal on an Instrument Landing System (ILS).

1. Introduction

Most of the real life environment can be approximated by hexahedral obstacles, or combinations of different hexahedral obstacles. Of course this leads to some artefacts like periodic radar cross section variations, the need for multiple diffractions to calculate the signal behind a cylindrical obstacle, or reflections that are ignored, because the approximated side plane is positioned so that a reflection on that plane can not reach the receiver (see Figure 1). To calculate the signal more accurately for those cases, we need to implement cylindrical obstacles into the EPICS program [1].

For each phenomenon, i. e., penetration, diffraction and reflection we briefly discuss the routines to find the intermediate (penetration, diffraction and/or reflection) points [2]. In most cases, this implies that we first solve

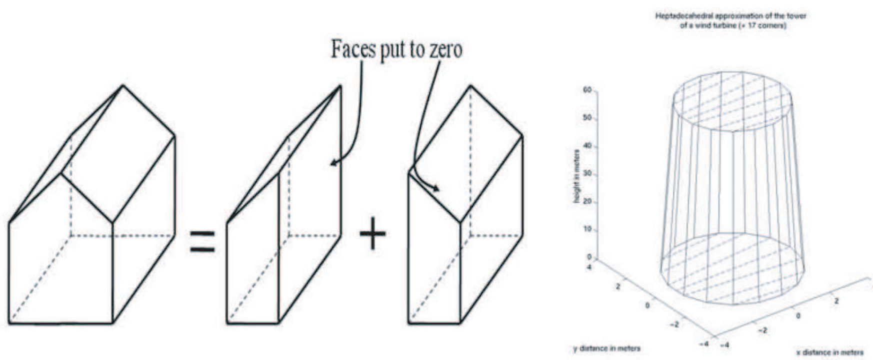

Figure 1: Examples of combinations of hexahedral obstacles to more complex obstacles house (left) and conical tower (right).

a two-dimensional problem which can be easily transformed to the three-dimensional solution. The main part of this paper, however, will be devoted to the electromagnetic computations of the field around these cylindrical obstacles.

1. Penetrations and Attenuation

In EPICS the "direct" field between 2 (intermediate) points is calculated in free space. However, this path might be obstructed by an obstacle. Therefore, each wall/obstacle obstructing this path introduces some attenuation of the signal strength. In general we have 3 possibilities: no penetration (e. g., the line transmitter-receiver is parallel to the axis of the cylinder but the distance between the two lines is bigger than the radius), one penetration (if either the transmitter or the receiver is inside the cylinder, while the other is outside, or in the tangent case) or two penetrations (general case).

1.1. How to Find the Penetration Points?

The routine to find the penetration points is rather easy: first we determine the crossing points of the line transmitter-receiver (or between 2 intermediate points) with the top and bottom plane of the cylinder. If these points are between the transmitter and receiver, and if the distance of these points to the centre of the top/bottom plane respectively is smaller than the radius of the cylinder, these are valid penetration points. The last step is to investigate the cylindrical wall. Therefore, we need to calculate the crossing points of the line between the projected locations of the transmitter and receiver and a circle. Figure 2 shows the side and top view of some examples (the transmitter is denoted by a $\diamond$, the receiver by a $\circ$ and the penetration point(s) by an $*$).

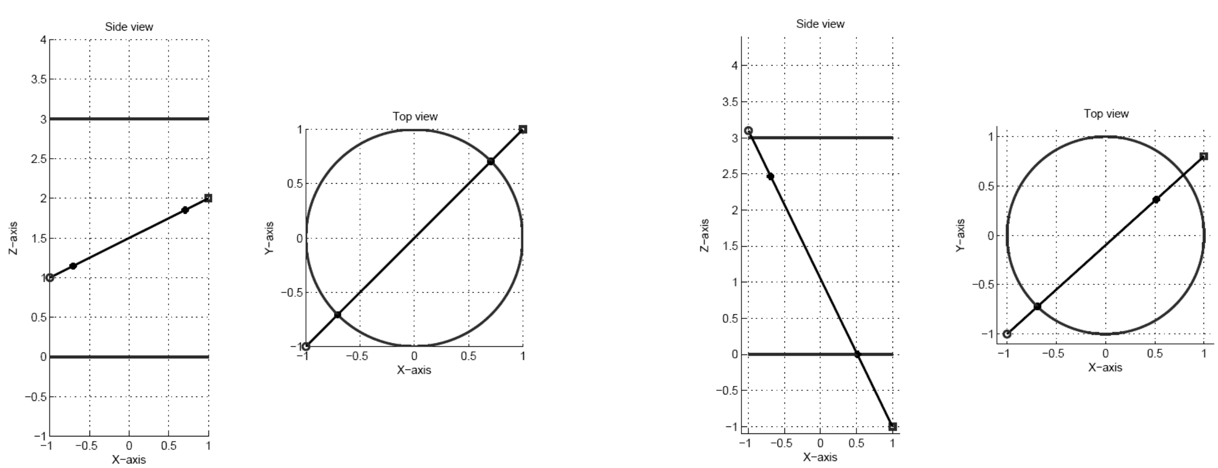

Figure 2: Examples of penetration: both through the side walls (left) and one penetration through a side wall combined with a penetration through the reference/bottom plane (right).

1.2. The GO Penetrated Field

Classical Geometrical Optics (GO) states that the high-frequency electromagnetic field propagates along ray paths, which satisfy the principle of Fermat, which states that the propagation of waves associated with these high frequency fields can be reduced to the study of wave paths along which the travel time is minimal. For perpendicular polarisation, the incident field lies in the plane perpendicular to the plane of incidence (soft boundary conditions). Hard boundary conditions require the incident field to be parallel with the plane of incidence. For the reflection by a non-perfectly electromagnetic conducting surface the plane-wave Fresnel reflection coefficients can be used:

$$\Gamma_{\perp} = \frac{\epsilon' \cos\theta - \sqrt{\epsilon - \sin^2\theta}}{\epsilon' \cos\theta + \sqrt{\epsilon - \sin^2\theta}}$$

$$\Gamma_{\parallel} = \frac{\cos\theta - \sqrt{\epsilon' - \sin^2\theta}}{\cos\theta + \sqrt{\epsilon' - \sin^2\theta}} \tag{1}$$

where θ is the angle between the incidence ray and the normal of the penetrated plane, ϵ the permittivity and σ the conductivity of the wall. Also the finite thickness of the wall under investigation can be taken into account if the dimensions are small with respect to the distance between transmitter and receiver. In those cases, a plane wave model based on successive reflections within the slab leads to much better results (Figure 3). Only when the losses are small and is not close to 1, edge effects have to be taken into account. However, for practical cases of concrete and thick walls the losses are sufficiently high.

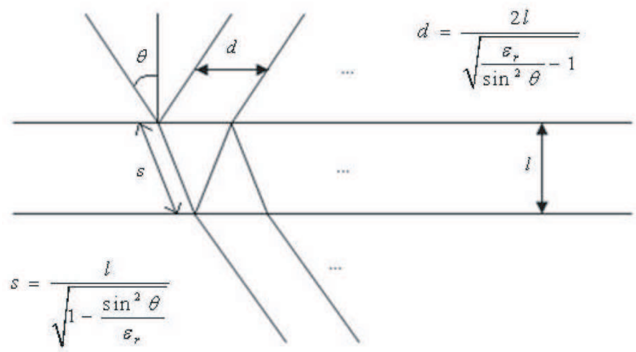

Figure 3: Multiple reflections within a slab.

If we suppose that walls can be approximated by a single slab of dielectric material we can easily see from (Figure 3) that the penetrated field is given by (2), where Γ is the appropriate reflection coefficient. Using this equation, the generalised transmission coefficient can be derived (3).

$$\vec{E}^t = \vec{E}^i \sum_{n=1}^{\infty} (1+\Gamma)(-\Gamma)^{2n-2}(1-\Gamma)\, e^{-2(n-1)s\alpha} e^{-2j(n-1)s\beta} e^{j(n-1)k_0 d \sin\theta} \tag{2}$$

$$\tau_g = \frac{\left(1-\Gamma^2\right) e^{-s\alpha} e^{-js\beta}}{\left(1-\Gamma^2\right) e^{-2s\alpha} e^{-j2s\beta} e^{jk_0 d \sin\theta}} \tag{3}$$

where k_0 denotes the free space phase constant, while α and β are the plane wave attenuation and phase constant of a lossy medium [3], given by (4). As for the case of the generalised reflection coefficient, the penetration coefficient for given material parameters may depend to a great extent on the frequency and thickness used. Inversely, when thickness and frequency are known penetration measurements can be used to estimate the material parameters of different structures [4].

$$\alpha = \omega \sqrt{\frac{\mu\epsilon}{2}} \sqrt{\sqrt{1 + \left(\frac{\sigma}{\omega\epsilon}\right)^2} - 1}$$

$$\beta = \omega \sqrt{\frac{\mu\epsilon}{2}} \sqrt{\sqrt{1 + \left(\frac{\sigma}{\omega\epsilon}\right)^2} + 1} \tag{4}$$

Figure 4 shows 2 examples of respectively a “perpendicular” incidence, where the line transmitter-receiver is perpendicular to the axis of the cylinder and a “non-perpendicular” incidence. In this last case an extra parameter m can be specified (note that the line transmitter-receiver is still crossing the axis of the cylinder).

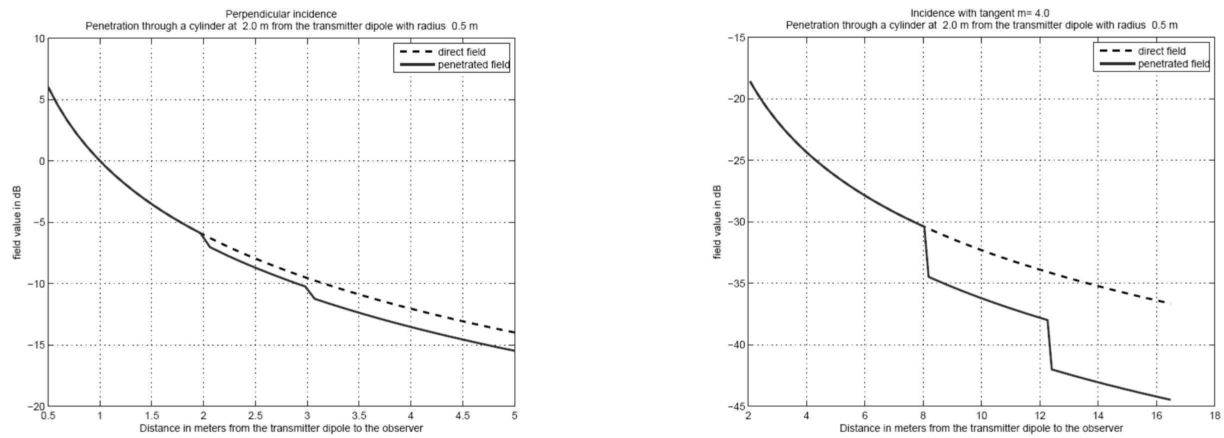

Figure 4: Examples of penetration through a cylinder: perpendicular (left) and non-perpendicular (right) case.

For these examples we used a wall with a thickness l of 0.1 m, a relative permittivity 2.5 (ϵ_r) and a conductivity of 0.036 (σ). The used frequency was 2.45 GHz.

Note that when m gets very high the losses through the faces are also bigger. For smaller incidence angles, resonance can occur in the wall, so that the losses are not directly proportional with s (see also Figure 3).

2. Diffractions

Again we can then solve the geometrical problem (see Figure 5). The determination of the diffraction points in a two-dimensional environment is rather easy: we draw the lines tangent to the circle from both the transmitter and the receiver (see top views). The last step is to determine which of the two points of the transmitter side corresponds with which point at the receiver side (smooth transmission between the air medium and the cylinder surface). Note that we only take diffractions around the cylinder into account. Thus, if one or both of the two diffraction points of one ray turns out to be above the "top" plane or below the "bottom" plane (reference plane), this ray is not taken into account (e. g., Figure 5).

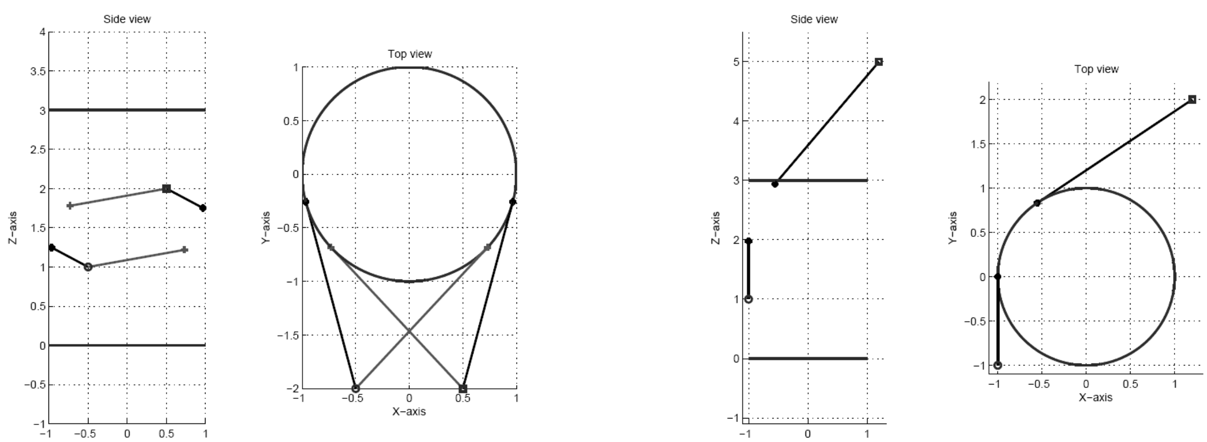

Figure 5: Examples of diffraction: both diffractions are valid (left) and the righter diffraction is ignored (right).

2.1. Vertical Polarisation

We have considered a plane wave incident upon a perfectly conducting cylinder (Figure 6). The incident wave is linearly polarised with electric vector $\vec{E^i}$ parallel to the axis of the cylinder. The incident $\vec{k}$-vector is perpendicular to the axis of the cylinder. In terms of cylindrical coordinates, we have

$$\vec{E^i} = \vec{i_z} E_0 e^{jkx} = \vec{i_z} E_0 e^{-jk\rho\cos\theta_0} \tag{5}$$

In this analysis we follow the procedure described by Kong [5].

To match the boundary conditions at $\rho = a$, we transform the plane wave solution into a superposition of cylindrical waves satisfying the Helmholtz wave equation in cylindrical coordinates:

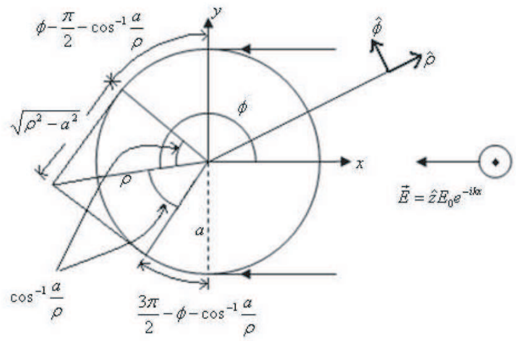

Figure 6: Scattering by a conducting cylinder.

$$e^{-jk\rho cos\theta_0} = \sum_{m=-\infty}^{\infty} a_m J_m(k\rho) e^{jm\phi} \tag{6}$$

The constant a_m can be determined by using orthogonality relations for $e^{jm\phi}$. We multiply both sides by $e^{-jn\phi}$ and integrate over ϕ from 0 to 2π. In view of the integral representation for the Bessel function,

$$J_n(k\rho) = \frac{1}{2\pi}\int_0^{2\pi} e^{-jk\rho cos\theta_0 - jn\phi + jn\pi/2} d\phi \tag{7}$$

we obtain $a_m = e^{-jn\pi/2}$ and

$$e^{-jk\rho cos\theta_0} = \sum_{m=-\infty}^{\infty} J_m(k\rho) e^{jm\phi - jm\pi/2} \tag{8}$$

This expression is referred to as the wave transformation, which represents a plane wave in terms of cylindrical waves.

The scattered wave can also be expressed as a superposition of the cylindrical functions satisfying the Helmholtz wave equation. Expecting outgoing waves, we write the solution in terms of Hankel functions of the first kind. The sum of the incident wave and the scattered wave satisfies the boundary condition of a vanishing tangential electric field at $\rho = a$. We find the total solution to be

$$\vec{E} = \vec{i_z} E_0 \sum_{n=-\infty}^{\infty} \left[J_n(k\rho) - \frac{J_n(ka)}{H_n^{(1)}(ka)} H_n^{(1)}(k\rho) \right] e^{jn\phi - jn\pi/2} \tag{9}$$

The first summation term represents the incident wave; the second summation term, the scattered wave. Note that for $\rho = a$, the field from (9) becomes zero. In the far-field zone, where $k\rho >> 1$, we can make use of the asymptotic formula for $H_n^{(1)}(k\rho)$ and find that the scattered wave takes the form of the first expression of (10) for small radii a, which can be expanded with respect to ka.

$$\vec{E}_s \approx \vec{i_z} E_0 \sum_{n=-\infty}^{\infty} \sqrt{\frac{2}{\pi k\rho}} \frac{J_n(ka)}{H_n^{(1)}(ka)} e^{jk\rho + jn(\phi - \pi) - j\pi/4}$$

$$\vec{E}_s = \vec{i_z} j E_0 \sqrt{\frac{2}{\pi k\rho}} \left[\frac{1}{ln(ka)} + (ka)^2 \cos\phi - \frac{(ka)^4}{8} \cos 2\phi + ... \right] e^{jk\rho - j\pi/4} \tag{10}$$

This series converges rapidly when the radius of the cylinder is small compared with the wavelength, $ka << 1$. The first term is angle-independent and signifies that the scattered wave caused by an infinitely thin wire is isotropic.

2.2. Horizontal Polarisation

We have also generalised the procedure and implemented the diffraction by a conducting cylinder for horizontal polarisation. In this case, the electrical field can be expressed like this (see Figure 6):

$$\vec{E^i} = \vec{i_y} E_0 e^{-jk\rho\cos\phi} \tag{11}$$

The scattered wave takes the following form:

$$\vec{E}_s = \vec{i_\rho} \sum_{n=-\infty}^{\infty} a_n H_n^{(1)}(k\rho) e^{jn(n-\pi/2)} + \vec{i_\phi} \sum_{n=-\infty}^{\infty} b_n H_n^{(1)}(k\rho) e^{jn(n-\pi/2)} \tag{12}$$

Once again, we have to require that the ϕ-component of the total field (incident and scattered field) vanishes for $\rho = a$.

The ϕ-component of the incident field (11) can be written as:

$$\begin{aligned} \vec{i_\phi} &= -\vec{i_x}\sin\phi + \vec{i_y}\cos\phi \\ \vec{E}^i_\phi &= -\vec{E_0}e^{-jk\rho\cos\phi}\cos\phi \end{aligned} \tag{13}$$

By differentiating Eq. (8) with respect to ρ we obtain:

$$-jke^{jk\rho\cos\phi} = k\sum_{n=-\infty}^{\infty} J'_n(k\rho)e^{-jn(n-\pi/2)} \tag{14}$$

where the derivative of the Bessel function can be found from [6]:

$$J'_n(z) = \frac{J_{n-1}(z) - J_{n+1}(z)}{2} \tag{15}$$

$$J'_0(z) = -J_1(z) \tag{16}$$

When considering only the ϕ-component of the scattered field (12), we find (17). Indeed, the ϕ-component vanishes in the far field. This expression can be simplified as we have done above for the vertical polarisation.

$$\vec{E} = \vec{i_\phi}E_0\sum_{n=-\infty}^{\infty}\left[J'_n(k\rho) - \frac{J'_n(ka)}{H^{(1)}_n(ka)}H^{(1)}_n(k\rho)\right]e^{jn(\phi-\pi/2)} \tag{17}$$

In Figure 7 both the vertical and horizontal component are shown for 2 examples. Note that the horizontal component gets stronger as the radius of the cylinder increases.

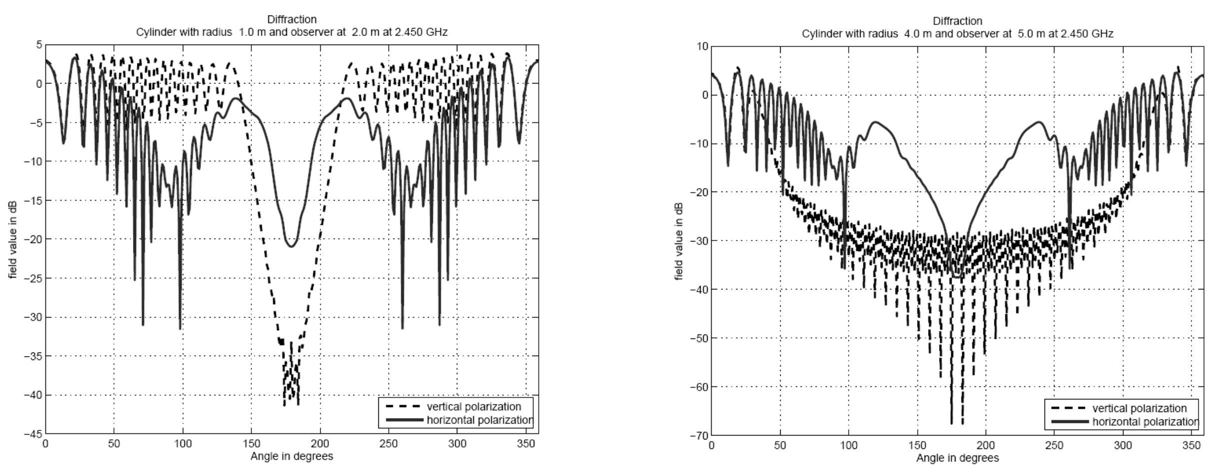

Figure 7: Examples of diffracted fields around a cylinder.

3. Reflections

3.1. Iterative Process Required to Find the Reflection Points

Whereas for the previous phenomena, the determination of the intermediate points was rather easy, this requires some more attention in the case of a reflection. Of course, one can determine some easy cases as well, e. g., reflections on top/bottom plane, symmetrical cases, etc. The general case for the determination of the reflection point(s), is somewhat more complicated. To find the solutions of the two-dimensional problem we have to solve a fourth degree equation iteratively [2]. This equation is derived by drawing a tangent line on the circle through a chosen reflection point on the circle to determine the mirror images of the transmitter (see Figure 8).

From those points, one can compute the points on the line transmitter-receiver (λ_2 and λ_2) where the signal will be reflected to (i. e., the crossing points between this line and the lines from the mirror image of the transmitter and the reflection points under investigation, determined by λ_1). The goal is to determine λ_1 so that the vector determined by λ_2, λ_{2b} respectively, is equal to the projection of the receiver. This implies that λ_2 and λ_{2b} should be equal to 1, leading to Eq. (18).

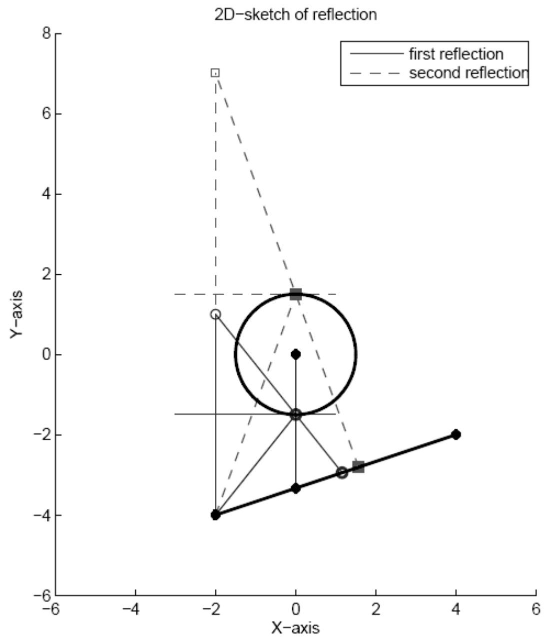

Figure 8: Sketch of general case.

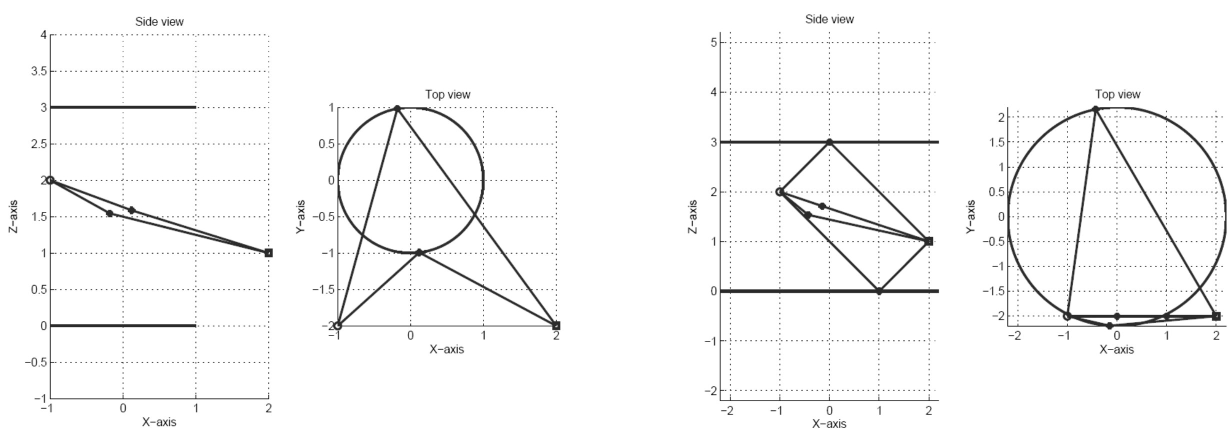

Figure 9: Examples of reflection on a cylinder: without (left) and with (right) reflections on the top and bottom plane.

$$\lambda_{2,2b} = \lambda_1 \left[\frac{\pm 2R_c\sqrt{a' + b'\lambda_1 + c'\lambda_1^2} - 2a' - b'\lambda_1}{\pm R_c\sqrt{a' + b'\lambda_1 + c'\lambda_1^2} - a' + c'\lambda_1^2} \right]$$
$$\lambda_{2,2b} = 1? \Leftrightarrow A_4\lambda_1^4 + A_3\lambda_1^3 + A_2\lambda_1^2 + A_1\lambda_1 + A_0 = 0 \tag{18}$$

where a' is the quadratic norm of the projected transmitter ($\lambda_1 = 0$), b' twice the scalar product between this vector and the vector between projected transmitter and receiver, c' the quadratic norm of this last vector and Rc the radius of the cylinder.

Unfortunately, we don't always have the possibility to solve a linear equation of the fourth order. Therefore, we will solve this problem iteratively by using the Newton-Raphson method. One can see that equation (18) has 4 possible singularities (nominator equal to zero), and that they are difficult to calculate (start value of Newton-Raphson has to be on the right side of these singularities). Therefore we will search a solution for the inverse function ($1/\lambda_2 = 1$). The last step will be again the transformation of the two-dimensional solution to the three-dimensional solution (excluding reflection points on the cylindrical wall that lie above the top plane or below the bottom plane).

3.2. Reflected Field Computations

For the implementation of the computation of the reflected field, one has to keep in mind that after the reflection, the location of the caustics, both for parallel and perpendicular to the axis of the cylinder, might have been changed as is shown in Figure 10.

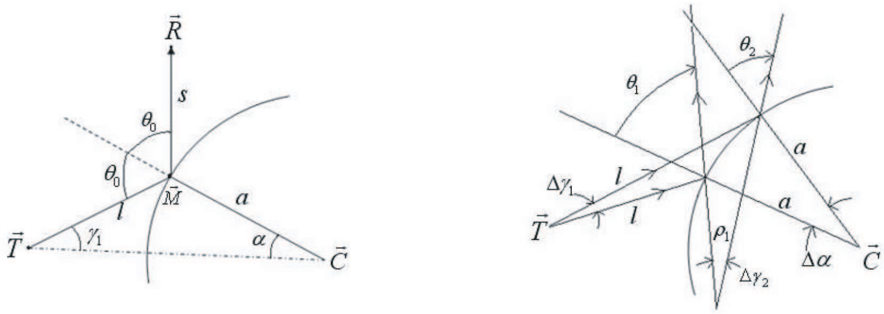

Figure 10: Reflection against a curved surface (parallel case).

Taking a cross-section along one of the radii of curvature, and expressing the arc on the circle as a function of the viewing angles, one can obtain:

$$a\Delta\alpha\cos\theta_0 = l\Delta\gamma_1 = \rho\Delta\gamma_2 \tag{19}$$

where $\Delta\gamma_1 = \Delta\theta_0 - \Delta\alpha$ and $\Delta\gamma_2 = \Delta\theta_0 + \Delta\alpha$. Eliminating $\Delta\alpha/\Delta\theta_0$ this leads to

$$\begin{aligned} \frac{1}{\rho_i} &= \frac{1}{l} + \frac{2}{R_i\cos\theta_0} \\ \frac{1}{R_1} &= \frac{\cos^2\alpha}{a} \\ \frac{1}{R_2} &= \frac{\sin^2\alpha}{a} \end{aligned} \tag{20}$$

where R_i represents the radius of curvature (parallel and perpendicular to the axis). Indeed, it can be shown in analysis that the radius of curvature of a function $y(x)$ is given by:

$$R_i = \frac{y''}{\sqrt{(1+y'^2)^3}} \tag{21}$$

In general the cut of a cylinder is an ellipse which can be expressed by $(x/a')^2 + (y/b')^2 = 1$, where $a' = a$ and $b' = a/\cos\alpha$, bearing in mind that α is the angle between the axis of the cylinder and the cut. Using (21) at the expression of the ellipse, one obtain the formulas of (20). Note that for the parallel case R_2 will become infinite. This implies that the distance to the new caustics can be computed:

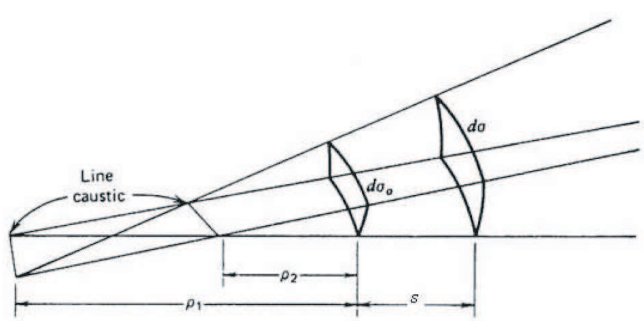

Figure 11: A bunch of rays with a different radius of curvature.

$$\begin{aligned} \frac{1}{\rho_1} &= \frac{1}{l} + \frac{2\cos^2\alpha}{a\cos\theta_0} \\ \frac{1}{\rho_2} &= \frac{1}{l} + \frac{2\sin^2\alpha}{a} \end{aligned} \tag{22}$$

Keeping in mind that the total distance after reflection is given by $d_i = \rho_i + s$, this implies that the field attenuation after reflection can be computed using:

$$|E| = |E_0| \sqrt{\frac{\rho_1 \rho_2}{(\rho_1 + s)(\rho_2 + s)}} \tag{23}$$

where $|E_0|$ is the field at reflection point $\vec{M}$. This attenuation has to be multiplied by the reflection coefficients which can be determined from the slab-approximation of the wall (see Figure 3).

$$\vec{E}^r = \vec{E}^i \left[\Gamma + \sum_{n=1}^{\infty} (1+\Gamma)(-\Gamma)^{2n-1}(1-\Gamma) e^{-2ns\alpha} e^{-2jns\beta} e^{jnk_0 d \sin\theta} \right] \tag{24}$$

$$\Gamma_g = \Gamma \left[1 - \frac{(1-\Gamma^2) e^{-2s\alpha} e^{-j2s\beta} e^{jk_0 d \sin\theta}}{(1-\Gamma^2) e^{-2s\alpha} e^{-j2s\beta} e^{jk_0 d \sin\theta}} \right] \tag{25}$$

3.3. Case Study: Brussels Airport Terminal

At Brussels airport, a few years ago a new terminal was build. This A-terminal has a curved shape, to reduce the influence on the Instrument Landing System (ILS) of the neighbouring runway. This ILS systems allows blind landings, and thus has to be very reliable. Using a curved shape, the effect of this new terminal was reduced radically. Figure 12 shows the effect of a rectangular building (left) and a curved building (right) on the differnce pattern of the ILS system (zero along the runway). Note that the buiding was approximated by a cylinder with a horizontal axis, which comes close to the current shape of this A-terminal. One can clearly see that in the zone where reflections can occur (between 3720 and 5200 m along the x-axis), the effect of the cylindrically shaped building is much smaller.

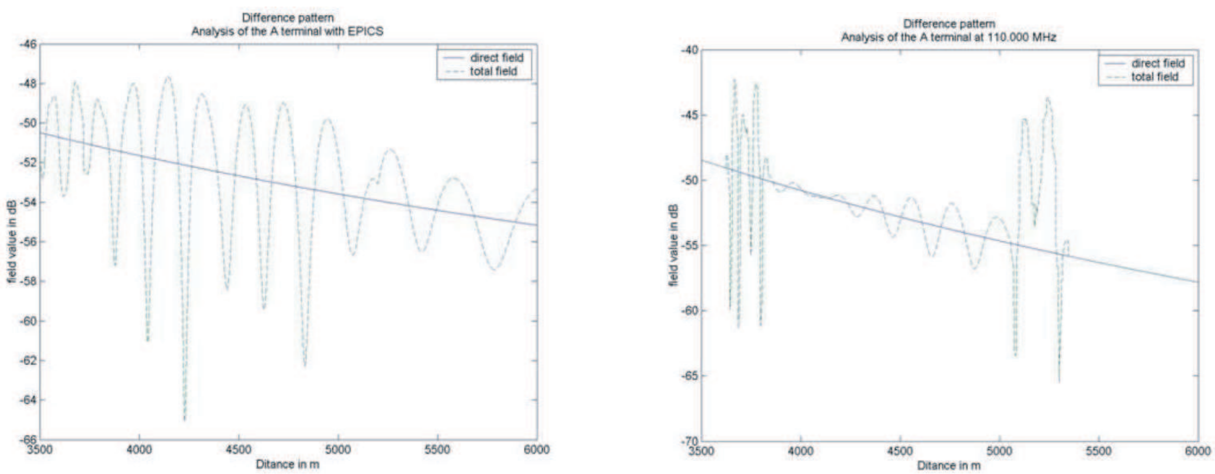

Figure 12: Comparsion between rectangular shaped (left) and curved shaped (right) A-terminal for the difference-pattern of the ILS system.

4. Conclusion

In this paper we investigated the influence of a cylindrical obstacle on the electromagnetic signal. Though it is not presented as a part of the EPICS software yet, new routines based on Geometric Optics (GO) have been written and tested to predict penetration, reflection and diffraction of electromagnetic fields around cylindrical obstacles as a step in a future implementation in EPICS.

Acknowledement

At the end of this paper, I would like to thank Rubèn Gonzàlez Gonzàlez for the implementation of these routines, during his master thesis.

REFERENCES

1. De Coster, I., "Deterministic propagation prediction for wireless communication systems," Ph. D. Thesis, K. U. Leuven, Leuven, Belgium, October 2000.

2. Trappeniers, D., E. van Lil, and A. van de Capelle, "UTD-GO implementation for cylindrical obstacles," *COST 273: Towards Mobile Broadband Multimedia Networks*, Paris, France, TD(03)104, May 2003.
3. Inan, U. S. and A. S. Inan, *Electromagnetic Waves*, Prentice Hall, Upper Saddle River, 2000.
4. Bellens, K., "Karakterisering van bouwmaterialen bij breedband communicatiefrequenties," Master thesis, K. U. Leuven, Belgium, May 1999 (Dutch).
5. Kong, J. A., *Electromagnetic Wave Theory*, AMW Publishing, 2000.
6. Abramovitz, M. and C. Stegun, *Handbook of Mathematical Functions with Formulas, Graphs and Mathematical Tables*, AMW Publishing, 2000.